

Measurement of carbonyl chemical shifts of excited protein states by relaxation dispersion NMR spectroscopy: comparison between uniformly and selectively ^{13}C labeled samples

Patrik Lundström · D. Flemming Hansen ·
Lewis E. Kay

Received: 18 July 2008 / Accepted: 18 July 2008 / Published online: 2 September 2008
© Springer Science+Business Media B.V. 2008

Abstract Carr–Purcell–Meiboom–Gill (CPMG) relaxation dispersion nuclear magnetic resonance (NMR) spectroscopy has emerged as a powerful method for quantifying chemical shifts of excited protein states. For many applications of the technique that involve the measurement of relaxation rates of carbon magnetization it is necessary to prepare samples with isolated ^{13}C spins so that experiments do not suffer from magnetization transfer between coupled carbon spins that would otherwise occur during the CPMG pulse train. In the case of ^{13}CO experiments however the large separation between ^{13}CO and $^{13}\text{C}^\alpha$ chemical shifts offers hope that robust ^{13}CO dispersion profiles can be recorded on uniformly ^{13}C labeled samples, leading to the extraction of accurate ^{13}CO chemical shifts of the invisible, excited state. Here we compare such chemical shifts recorded on samples that are selectively labeled, prepared using $[1-^{13}\text{C}]$ -pyruvate and $\text{NaH}^{13}\text{CO}_3$, or uniformly labeled, generated from ^{13}C -glucose. Very similar ^{13}CO chemical shifts are obtained from analysis of CPMG experiments recorded on both samples, and comparison with chemical shifts measured using a second approach establishes that the shifts measured from relaxation dispersion are very accurate.

Keywords Relaxation dispersion NMR · Chemical exchange · Carr–Purcell–Meiboom–Gill · Excited protein states · Chemical shifts

Abbreviations

NMR Nuclear magnetic resonance
CPMG Carr–Purcell–Meiboom–Gill

Introduction

Nuclear magnetic resonance (NMR) spectroscopy is a powerful tool for the study of protein dynamics on the millisecond time scale—a regime that is important for a wide range of biological functions that include folding (Hill et al. 2000; Korzhnev et al. 2004; Sugase et al. 2007; Zeeb and Balbach 2005), enzyme catalysis (Boehr et al. 2006; Eisenmesser et al. 2002, 2005; Vallurupalli and Kay 2006; Watt et al. 2007; Wolf-Watz et al. 2004) and ligand binding (Mulder et al. 2001; Sugase et al. 2007). In particular, Carr–Purcell–Meiboom–Gill (CPMG) (Carr and Purcell 1954; Meiboom and Gill 1958) relaxation dispersion experiments are extremely well suited to characterize these motions as they are sensitive to both the rate constants that describe the exchange process and to the chemical shifts of exchanging states, so long as the populations of such states exceed approximately 0.5% (Palmer et al. 2001, 2005). The experiments are based on monitoring the line-widths of NMR signals as a function of the frequency of refocusing pulses applied during a constant-time relaxation delay (Loria et al. 1999; Tollinger et al. 2001).

In cases where the exchanging states are low populated and only transiently formed they become ‘invisible’ to the tools of structural biology and their structures become very

P. Lundström · D. F. Hansen · L. E. Kay (✉)
Department of Medical Genetics, The University of Toronto,
Toronto, ON, Canada M5S 1A8
e-mail: kay@pound.med.utoronto.ca

P. Lundström · D. F. Hansen · L. E. Kay
Department of Biochemistry, The University of Toronto,
Toronto, ON, Canada M5S 1A8

P. Lundström · D. F. Hansen · L. E. Kay
Department of Chemistry, The University of Toronto, Toronto,
ON, Canada M5S 1A8

difficult to probe. In this regard, the chemical shifts obtained from CPMG relaxation dispersion experiments are extremely important. For example, it is well known that chemical shifts encode structural information (Spera and Bax 1991; Wishart and Sykes 1994), with different nuclei reporting on unique aspects of structure. The chemical shifts of backbone amide ^{15}N spins, for instance, are sensitive in a complex way to ϕ_i/ψ_{i-1} , χ_i^1 and χ_{i-1}^1 dihedral angles as well as to hydrogen bond lengths, while chemical shifts of ^1HN spins primarily depend on ϕ_i/ψ_{i-1} , hydrogen bond lengths and solvent accessibilities (Le and Oldfield 1994; Neal et al. 2003; Shen and Bax 2007; Xu and Case 2002). Other nuclei, like $^1\text{H}^\alpha$, $^{13}\text{C}^\alpha$, $^{13}\text{C}^\beta$ and ^{13}CO are more direct reporters of secondary structure and are primarily sensitive to ϕ_i/ψ_i dihedral angles (Ando et al. 1984; Spera and Bax 1991; Wishart and Case 2002), although $^1\text{H}^\alpha$ shows additional dependence on ring current effects (Neal et al. 2003; Wishart and Case 2002) and hydrogen bonding (Pardi et al. 1983; Wagner et al. 1983; Wishart et al. 1991).

Chemical shift information can be incorporated into structure calculations through dihedral angle restraints that are obtained by searching a protein structure database for fragments that are compatible with the experimental shifts (Cornilescu et al. 1999). These restraints are normally combined with other types of data such as nuclear Overhauser enhancements (NOE), residual dipolar couplings (RDCs) and residual chemical shift anisotropies (RCSA) to produce high quality structures (Bax 2003; Prestegard et al. 2005; Tjandra and Bax 1997; Tolman et al. 1995). Very recently protocols have been developed whereby chemical shifts of ^{15}N , ^1HN , ^{13}CO , $^{13}\text{C}^\alpha$, $^{13}\text{C}^\beta$ and $^1\text{H}^\alpha$ are used in concert with databases to produce structures of small proteins (≤ 150 residue) that are in remarkably good agreement with those calculated by conventional NMR methods or by X-ray crystallography (Cavalli et al. 2007; Shen and Bax 2007). In a related manner we have calculated a high resolution backbone fold for an invisible excited state that corresponds to the ligand bound form of an SH3 domain (Vallurupalli et al. 2008b), based on input data from relaxation dispersion experiments, including ^{15}N , ^1HN , ^{13}CO and $^{13}\text{C}^\alpha$ chemical shifts (Hansen et al. 2008c) and anisotropic restraints in the form of $^1\text{HN}-^{15}\text{N}$ (Vallurupalli et al. 2007), $^1\text{H}^\alpha-^{13}\text{C}^\alpha$, $^1\text{HN}-^{13}\text{CO}$ RDCs (Hansen et al. 2008b) and ^{13}CO RCSAs (Vallurupalli et al. 2008a).

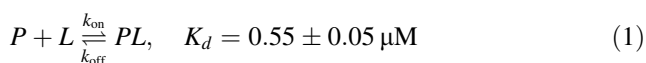
Key to the approach has been the development of isotope labeling methodologies that generate isolated spin-systems that can be probed in an artifact free manner by relaxation dispersion CPMG methods. This is readily accomplished in the case of experiments that involve measurement of ^{15}N chemical shifts and $^1\text{H}-^{15}\text{N}$ RDCs of invisible states since nitrogen spins are effectively isolated from each other in a uniformly ^{15}N labeled protein. The situation is more complex in the case of applications to studies involving ^{13}C . Use of

uniform labeling leads to the presence of large $^1J_{\text{CC}}$ couplings (35–55 Hz) that potentially can have serious consequences for the accurate extraction of ^{13}C based chemical shifts, ^{13}C -X RDCs and ^{13}C RCSAs from CPMG-based relaxation dispersion experiments. The obvious way to mitigate this problem is to use selective labeling schemes where as many as possible of the problematic couplings are removed, while maintaining a high level of ^{13}C enrichment at the desired positions. Labeling protocols based on [1- ^{13}C]- and [2- ^{13}C]-glucose (Lundström et al. 2007; Teilmann et al. 2006), [3- ^{13}C]-pyruvate (Ishima et al. 2001; Lee et al. 1997; Mulder et al. 2002), [1,3- $^{13}\text{C}_2$]- and [2- ^{13}C]-glycerol (LeMaster and Kushlan 1996) and mixtures of labeled and unlabeled acetate (Wand et al. 1995) have been described. Recently, we have shown that accurate $^{13}\text{C}^\alpha$ chemical shifts and $^1\text{H}^\alpha-^{13}\text{C}^\alpha$ RDC values of invisible states can be extracted from molecules labeled with [2- ^{13}C]-glucose (Hansen et al. 2008c; Korzhnev et al. 2007), while robust measures of ^{13}CO shifts, ^{13}CO RCSA values and $^1\text{HN}-^{13}\text{CO}$ RDCs have been reported from dispersion experiments recorded on proteins labeled with isolated ^{13}CO probes using [1- ^{13}C]-pyruvate and $\text{NaH}^{13}\text{CO}_3$ as carbon sources (Hansen et al. 2008c).

There are, however, obvious disadvantages with selective isotope labeling schemes. Among these are (i) that it is usually not feasible to label a particular position in all residue types without resorting to unrealistically complicated and expensive combinations of precursors, (ii) that many attractive precursors lead only to fractional enrichment at the desired positions, (iii) that many carbon sources result in slow bacterial growth and low levels of protein over-expression, and finally (iv) that in general it is more time- and cost-efficient if the same protein sample can be used for many types of experiments. Therefore, it is worthwhile to explore situations where ^{13}C dispersion experiments can be performed using uniformly labeled samples that have become ubiquitous in modern biological NMR applications. The natural place to start is with the backbone ^{13}CO spin since it resonates sufficiently downfield in the carbon spectrum so that it can be excited by means of selective pulses that do not perturb aliphatic carbon spins. Indeed, ^{13}CO dispersion experiments have been recorded on uniformly ^{13}C labeled samples previously by Ishima et al. in the context of a study of millisecond time-scale motions in the HIV-1 protease. While there was general agreement as to the regions in the protein that showed ms time-scale dynamics using both ^{15}N - and ^{13}CO -based experiments (Ishima et al. 2004), the accuracy of the extracted ^{13}CO chemical shifts was not established. The authors did note, however, that for at least one Asn residue there was significant oscillation in the dispersion profile that was due to a substantial $^3J_{\text{CO},\text{C}\gamma}$ coupling. Extensive simulations that they performed showed that for constant-time relaxation delays ≤ 32 ms and $J_{\text{CO},\text{C}}$ couplings less

than 2.5 Hz the resulting errors in the ^{13}C O transverse relaxation rates were small ($<0.5\text{ s}^{-1}$).

In what follows we first present a comparison of the extent of ^{13}C O labeling achieved using the ^{13}C precursors [$1\text{-}^{13}\text{C}$]-pyruvate and $\text{NaH}^{13}\text{CO}_3$ that generate ‘isolated’ ^{13}C O spin systems that highlights some of the limitations associated with specific labeling, as described above. In order to establish whether such a labeling scheme is justified, the accuracies of ^{13}C O chemical shifts of the excited state that are extracted from relaxation dispersion experiments recorded on a sample with ‘isolated’ ^{13}C O spins (Hansen et al. 2008c) are compared to those obtained presently from measurements recorded on a uniformly ^{13}C labeled sample. Here we use an exchanging system that has been described previously (Hansen et al. 2008c; Vallurupalli et al. 2007) based on the binding reaction,



where P and L correspond to the SH3 domain from the yeast protein Abp1p (Drubin et al. 1990; Lila and Drubin 1997; Rath and Davidson 2000) and a 17 residue binding peptide from the protein Ark1p (Haynes et al. 2007), respectively. The addition of only a small mole fraction of L ($\approx 5\%$) ensures that PL is the invisible, ‘excited’ state, while P remains the visible, ‘ground’ state whose resonances are observed in NMR spectra. The ^{13}C O chemical shift differences (between P and PL) that are measured from CPMG experiments can subsequently be compared to those obtained directly from measurements on samples comprising only P (no L) or PL (saturating amounts of L) and in this manner the accuracy of the chemical shifts of the excited state can be quantified. We show here that very accurate ^{13}C O chemical shifts can be obtained using uniformly ^{13}C -labeled samples, and that accuracy is not sacrificed relative to experiments performed on samples where the ^{13}C O spins are isolated. There are thus distinct advantages to using uniformly ^{13}C labeled samples in ^{13}C O relaxation dispersion studies.

Materials and methods

Protein sample preparation

Abp1p SH3 domains were isotopically enriched by protein expression in BL21(DE3) cells grown in M9 minimal media supplemented with $^{15}\text{NH}_4\text{Cl}$ as the sole nitrogen source and with the appropriate carbon source, depending on the sample. Production of a $^{15}\text{N}/^{13}\text{C}$ O enriched sample (isolated ^{13}C O spins; sample 1) was achieved using 2.5 g/l [$1\text{-}^{13}\text{C}$]-pyruvate and 3 mM ($\sim 0.25\text{ g/l}$) $\text{NaH}^{13}\text{CO}_3$ as the carbon sources.

Cells were grown to OD 0.8 and protein expression induced with 1 mM IPTG. At this point 7 mM $\text{NaH}^{13}\text{CO}_3$ was added

and the cells were grown for 7 h at 37°C. Production of a highly deuterated, U- ^{15}N , ^{13}C labeled sample (sample 2) was achieved using [$\text{U-}^{13}\text{C}_6$, $^2\text{H}_7$]-glucose in 99.9% $^2\text{H}_2\text{O}$. Note that a deuterated sample is not required for the experiments performed here but was necessary for a separate application. A 17 residue Ark1p peptide (primary sequence: KKTKPT PPPKPSHLKPK) was expressed as described previously (Vallurupalli et al. 2007). The Abp1p SH3 domains and the unlabeled Ark1p peptide were purified according to Vallurupalli et al. (2007). Samples were prepared in 50 mM sodium phosphate, 100 mM NaCl, 2 mM EDTA, and 2 mM NaN_3 , pH 7.0 buffer, 10% D_2O , with protein concentrations of approximately 0.9 mM. An exchanging $P + L \leftrightarrow PL$ sample was prepared by titrating Ark1p peptide into a solution of the SH3 domain so that $[\text{PL}]/([\text{P}] + [\text{PL}]) = 6\%$ as determined by ^{15}N CPMG experiments.

NMR spectroscopy

All NMR experiments were performed at 25°C on Varian Inova spectrometers with ^1H resonance frequencies of 600 and 800 MHz, equipped with cold and room temperature probeheads, respectively. The fractional ^{13}C enrichment at CO positions in the ^{13}C O selectively labeled sample was determined by comparing the intensities of resonances in ^{15}N -HN planes of HNCOSY spectra (Kay et al. 1990) of a sample produced using [$1\text{-}^{13}\text{C}$]-pyruvate and $\text{NaH}^{13}\text{CO}_3$ with intensities of correlations from spectra of a sample generated using uniformly ^{13}C labeled glucose. To account for different sample concentrations the intensities were normalized by the average signal intensity in $^1\text{HN-}^{15}\text{N}$ HSQC data sets since all proteins were U- ^{15}N labeled. The fractional enrichment at position i is defined as $E_i = (C_{s,i}/N_s)/(C_{u,i}/N_u)$, where $C_{s,i}$ and $C_{u,i}$ are the peak intensities of resonance i in HNCOSY data sets of the selectively and uniformly labeled samples, respectively, that were recorded identically, N_s and N_u are normalization factors corresponding to the average of peak intensities in $^1\text{HN-}^{15}\text{N}$ HSQC data sets of the different samples.

^{13}C O CPMG relaxation dispersion experiments were recorded at 600 and 800 MHz on a highly deuterated sample comprised of U- ^{15}N , ^{13}C Abp1p SH3 domain, $\approx 6\%$ unlabeled Ark1p peptide, using a pulse sequence described herein (Fig. 2). Datasets recorded without the $^3J_{\text{CO,CO}}$ refocusing element of Fig. 2 (inset; see below) were obtained with $T_{\text{relax}} = 30\text{ ms}$, ν_{CPMG} values between 33 and 933 Hz and N any integer (see Fig. 2), while datasets with the refocusing element were recorded with $T_{\text{relax}} = 40\text{ ms}$, values of ν_{CPMG} between 50 and 900 Hz and even values for N . In all cases a total of 20 2D planes were recorded and the total experimental time for each complete dispersion dataset was 15 h at both 600 and 800 MHz.

Data sets were processed and analyzed with the nmrPipe/nmrDraw suite of programs (Delaglio et al. 1995) and

SPARKY (Goddard and Kneller), with peak intensities quantified using the program FuDA (available upon request). CPMG relaxation dispersion profiles, $R_{2,\text{eff}}(v_{\text{CPMG}})$ versus v_{CPMG} , were calculated as $R_{2,\text{eff}}(v_{\text{CPMG}}) = -\ln(I(v_{\text{CPMG}})/I_0)/T_{\text{relax}}$, where $I(v_{\text{CPMG}})$ is the peak intensity for different v_{CPMG} values and I_0 is the peak intensity obtained when the CPMG block is omitted. Here $v_{\text{CPMG}} = 1/(4\tau_{\text{CP}})$, where $2\tau_{\text{CP}}$ is the interval between successive 180° refocusing pulses during the CPMG element. Uncertainties in $R_{2,\text{eff}}(v_{\text{CPMG}})$ values were chosen on the basis of duplicate measurements. All dispersion data were fitted to a two-state model of chemical exchange. In order to establish which residues should be included in such fits, all dispersion profiles were initially fit on a per-residue basis to models that either include or do not include chemical exchange; in the former case global exchange parameters corresponding to the population of the excited state, p_B , and $k_{\text{ex}} = k_{\text{on}}[L] + k_{\text{off}}$, were fixed to the values determined from ^{15}N CPMG dispersion experiments recorded on the same sample. Residues were retained for further analysis if fits using the two-site exchange model were significant as established by F -test analyses, with $p < 0.01$. A total of 32 residues were retained in this manner. Dispersion profiles for Ser 52 were excluded since chemical exchange was detected for this residue in the apo SH3 domain.

^{13}C chemical shifts for the free SH3 domain as well as for the SH3 domain-Ark1p peptide complex (completely bound) were determined from ^{13}C - ^1H N slices of HNC0 experiments and subsequently compared with shift differences isolated from relaxation dispersion experiments that were obtained on the basis of a global analysis of the dispersion data that included 31 residues for which chemical exchange could be quantified reliably (see above).

Chemical shift differences from fits of ^{13}C relaxation dispersion profiles recorded on a ^{13}C -selectively labeled sample have been obtained previously, as described by Hansen et al. (2008c), and were used in some of the analyses reported here.

Results and discussion

In previous studies from our laboratory that included measurement of ^{13}C chemical shifts, ^{13}C RCSAs and two-bond ^1H - ^{13}C RDC values in an excited state corresponding to the Ark1p peptide bound form of the Abp1p SH3 domain, samples with isolated ^{13}C labeling at the carbonyl position were prepared from $[1-^{13}\text{C}]$ -pyruvate and $\text{NaH}^{13}\text{CO}_3$ (Hansen et al. 2008b, c; Vallurupalli et al. 2008a). Our initial thinking was that ^{13}C dispersion experiments recorded on samples generated in this manner would be ‘cleaner’ than the corresponding experiments performed on fully labeled samples since artifacts from evolution due to ^{13}C - ^{13}C scalar couplings

during the CPMG relaxation element would be minimized. Indeed we were able to show that very accurate values of chemical shifts of the excited state could be extracted using selectively labeled samples, but at the expense of incomplete or absence of labeling for several residues. In order to place the advantages of U- ^{13}C labeled samples in perspective, we first describe the levels of ^{13}C labeling that are expected using a strategy based on $[1-^{13}\text{C}]$ -pyruvate and $\text{NaH}^{13}\text{CO}_3$ based on an analysis of metabolic pathways for the 20 amino acids. Subsequently the experimentally determined levels of incorporation using this selective labeling approach are presented, that illustrate that substantial improvements in signal-to-noise can be achieved in studies using uniformly ^{13}C labeled samples. Finally and most important we show that accurate ^{13}C chemical shifts can be extracted from U- ^{13}C labeled samples using optimized pulse schemes that include ^{13}C refocusing pulses during the CPMG element that have been designed to minimize excitation of aliphatic spins.

Incorporation of ^{13}C into carbonyl positions of amino acids prepared from $[1-^{13}\text{C}]$ -pyruvate and $\text{NaH}^{13}\text{CO}_3$

The main metabolic pathways for the biosynthesis of amino acids are well established and described in detail in elementary biochemistry textbooks (Voet and Voet 1995). Here we present a brief synopsis that allows the reader to understand how label is incorporated when using the simple (and commercially available) compounds $[1-^{13}\text{C}]$ -pyruvate and $\text{NaH}^{13}\text{CO}_3$.

The amino acid backbones are synthesized from a small set of precursors, including pyruvate (Ala, Lys, Val) and the related molecules phosphoenolpyruvate (PEP) (Phe, Tyr), 3-phosphoglycerate (3PG) (Cys, Gly, Ser, Trp), oxaloacetate (OA) (Asn, Asp, Met, Lys, Thr), α -ketoglutarate (AKG) (Arg, Gln, Glu, Pro), acetyl-S-CoenzymeA (Ac-S-CoA) (Leu) and ribose-5-phosphate (R5P) (His). Note that the backbone of Lys may be synthesized from two different precursors because of the symmetric intermediate L,L- α,ϵ -diaminopimelate (Voet and Voet 1995) that is made up of equivalent halves, one derived from pyruvate and one from OA.

Figure 1 illustrates that if glycolysis is the major metabolic pathway and using $[1-^{13}\text{C}]$ -pyruvate and $\text{NaH}^{13}\text{CO}_3$ as the sole carbon precursors, enrichment levels of 100% are expected at CO positions for amino acids derived from pyruvate, PEP and 3PG with no incorporation of label at C^α positions. It is also clear that the amino-acids derived from OA can be enriched at CO, without labeling at C^α , if PEP is carboxylated to yield OA since position 1 of OA directly becomes the carbonyl position of these residues. However, OA is also synthesized by the TCA cycle and, as shown in Fig. 1, even a single pass through the TCA cycle inevitably leads to decarboxylation of the labeled position and the

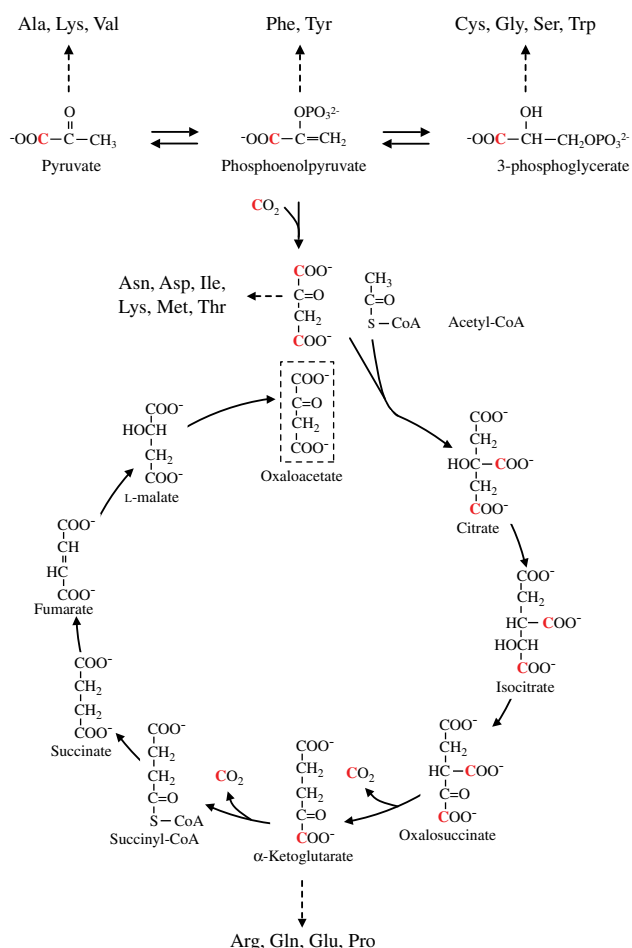


Fig. 1 Biosynthetic pathways showing the mechanism of ^{13}C enrichment at CO positions when $[1-^{13}\text{C}]$ -pyruvate and $\text{NaH}^{13}\text{CO}_3$ are used as carbon sources. Enriched positions are shown in red. Lys is shown twice since its backbone can be derived from either pyruvate or oxaloacetate. The pathways for biosynthesis of His and Leu are not shown since these amino acids are not enriched at CO using this labeling scheme

production of OA that is unlabeled. The amount of enrichment for OA derived amino acids is, therefore, ultimately a function of the rate of carboxylation of PEP and its direct incorporation into amino acids relative to flux of OA into the TCA cycle that leads to dilution of label. The TCA cycle intermediate AKG is the precursor for Arg, Gln, Glu and Pro. Position 1 of AKG corresponds to position 4 of OA, which is readily labeled if $^{13}\text{CO}_2$, supplied in the form of $\text{NaH}^{13}\text{CO}_3$, is used to carboxylate PEP. This leads to enrichment at CO but not C^α of these residues, but this label is lost when AKG is decarboxylated to succinyl-S-CoA so that only the first pass through the TCA cycle is productive for labeling CO for AKG derived amino acids. The use of $[1-^{13}\text{C}]$ -pyruvate and $\text{NaH}^{13}\text{CO}_3$ as carbon sources thus leads to enrichment at CO in 18 out of the 20 amino acids. The exceptions are His, where CO is derived

from position 5 of R5P, and Leu, where CO is derived from position 1 of Ac-S-CoA.

We have quantified the levels of enrichment at CO positions from this labeling scheme ($[1-^{13}\text{C}]$ -pyruvate and $\text{NaH}^{13}\text{CO}_3$ precursors) by producing a sample of $^{15}\text{N},^{13}\text{C}$ labeled Abp1p SH3 domain and a second Abp1p SH3 domain sample that is U- $^{15}\text{N},^{13}\text{C}$ labeled. Ratios of peak intensities that have been measured in $^{15}\text{N}-^1\text{HN}$ planes of HNCQ experiments recorded on both samples provide estimates of the degree of labeling, once differences in sample concentrations are accounted for by normalizing by averages of peak intensities in $^1\text{HN}-^{15}\text{N}$ HSQC data sets recorded on the two samples (see “Materials and methods”). The results from such an analysis are presented in Table 1 and the agreement with predictions is good. For residues where the backbone is derived from pyruvate, PEP and 3PG, enrichments of ^{13}C at the CO position range from 0.71 to 0.95. Enrichments less than 1.0 are obtained due to additional pathways that ultimately yield unlabeled pyruvate, most importantly the pentose phosphate pathway. It is noteworthy that the residues derived from 3PG are enriched to a smaller degree than those derived from pyruvate or PEP. This can be explained by the fact that Gly may also be derived from Thr which is only enriched at a level of 25% and that once formed Gly can be converted to Ser by addition of a methylene group from $\text{N}^5, \text{N}^{10}$ -methylene-THF (Voet and Voet 1995) and then further to Cys and the backbone of Trp. Furthermore, enrichment levels for Ala and Val differ by $\approx 10\%$ although both are supposedly synthesized from pyruvate. This implies that Ala may be produced in ways other than by transamination of pyruvate. Indeed, Ala can also be obtained by desulfuration of Cys via a pathway that makes available sulfur for the synthesis of various molecules (Mihara and Esaki 2002) and by degradation of Trp (Voet and Voet 1995). As expected, the enrichments for residues derived from OA and AKG are substantially lower, 24–31%, indicating a significant flux through the TCA cycle that results in loss of label. It is noteworthy that the enrichment of residues from both groups is similar, which indicates that the carbon dioxide present in the cells is predominantly ^{13}C labeled when $[1-^{13}\text{C}]$ -pyruvate and $\text{NaH}^{13}\text{CO}_3$ are the carbon sources. As expected we could not detect any enrichment at the CO positions of Leu and although His could not be quantified since it is not present in the Abp1p SH3 domain it is also not expected to be ^{13}C enriched at CO.

In agreement with predictions, incorporation of ^{13}C label at C^α is almost zero. For the sample used to calculate the yields above, there is absolutely no evidence of $^{13}\text{CO}-^{13}\text{C}^\alpha$ spin pairs that would manifest as a superposition of doublets separated by 55 Hz (corresponding to a $^{13}\text{CO}-^{13}\text{C}^\alpha$ spin pair) and singlets (corresponding to an isolated ^{13}CO) in $^{13}\text{CO}-^1\text{HN}$ planes of HNCQ data sets

Table 1 ^{13}C enrichment levels at CO positions using $[1-^{13}\text{C}]$ -pyruvate and $\text{NaH}^{13}\text{CO}_3$ as carbon sources

Precursor	Residue	Enrichment
Pyruvate	Ala	0.84 ± 0.02 (4)
	Val	0.95 ± 0.02 (3)
Phosphoenolpyruvate	Phe	0.85 ± 0.02 (2)
	Tyr	0.83 ± 0.01 (3)
3-Phosphoglycerate	Cys ^a	n.a.
	Gly ^b	0.71 ± 0.1 (4)
	Ser	0.71 ± 0.02 (3)
	Trp	0.78 ± 0.03 (3)
Oxaloacetate	Asn	0.24 ± 0.008 (4)
	Asp	0.24 ± 0.007 (8)
	Ile	0.31 ± 0.004 (3)
	Met	$0.31 \pm \text{n.a.}$ (1)
α -Ketoglutarate	Thr	0.25 ± 0.0005 (2)
	Arg ^a	n.a.
	Gln ^a	n.a.
	Glu	0.25 ± 0.006 (7)
Oxaloacetate or pyruvate	Pro	0.26 ± 0.006 (2)
	Lys	0.63 ± 0.009 (3)
Acetyl-S-CoA	Leu	0 ± 0 (5)
Ribose-5-phosphate	His ^a	n.a.

^a These residue types are not present in the SH3 domain of Abp1p that was used in the analysis

^b The large standard deviation for Gly is due to residue Gly39 for which an enrichment of 0.87 was quantified. Removal of this residue from the analysis gives a ^{13}C enrichment for Gly of 0.66 ± 0.03

recorded without decoupling of $^{13}\text{C}^\alpha$ during the ^{13}CO evolution period. Interestingly, a previously prepared sample showed a small fraction of ^{13}CO – $^{13}\text{C}^\alpha$ spin pairs (<2%) for residues derived from pyruvate, PEP and 3PG (Hansen et al. 2008c), although ^{13}CO – $^{13}\text{C}^\alpha$ spin pairs were not observed for Asn, Asp, Met or Thr. The main difference in the growth protocols for the two samples was that over-expression was carried out at 37° for 7 h for the protein used in the present study, instead of overnight at room temperature. It is thus plausible that shorter periods of over-expression lead to less scrambling of label and thus less enrichment at unexpected positions. Indeed, in keeping with this theme extremely faint peaks corresponding to ^{13}CO of Leu were clearly visible in spectra recorded on the sample prepared with the longer over-expression time.

The labeling scheme described above is highly selective, in large part because the labeled positions of OA are decarboxylated even after a single pass through the TCA cycle and because Ac-S-CoA also is unlabeled. An additional enriched position however is C^γ of the amino acids derived from OA. Because of very similar enrichments at CO for residues derived from OA and AKG (see above),

the fraction of ^{13}CO labeled amino acids that are simultaneously ^{13}C labeled at C^γ is likely to be large. As mentioned previously, this can be problematic for Asx residues (Ishima et al. 2004) but potentially of use in the case of Thr and Ile since it becomes possible to obtain isolated Thr $^{13}\text{C}^{\gamma 2}$ and Ile $^{13}\text{C}^{\delta 1}$ (which is derived from Thr $\text{C}^{\gamma 2}$) methyl groups by using a growth medium with $[\text{U}-^{12}\text{C}_6]$ -glucose and $\text{NaH}^{13}\text{CO}_3$ as carbon sources. We quantified the incorporation at these positions to be 0.29 ± 0.009 (3) for Ile and 0.28 ± 0.004 (2) for Thr.

In principle it should be possible to obtain significantly higher enrichments at the CO positions for the amino acids derived from OA and AKG by using bacteria with lesions in the TCA cycle so that all amino acids produced from these precursors are always enriched at CO (LeMaster and Kushlan 1996). This is possible, in principle, by knocking out the genes coding for malate dehydrogenase (malate to oxaloacetate in Fig. 1) and succinate dehydrogenase (succinate to fumarate in Fig. 1) in BL21 (DE3) cells. However, although such cells grow well on glucose, growth is unacceptably slow when pyruvate is used as the carbon source and we did not pursue this strategy further.

The above analysis establishes that while isolated ^{13}CO label can be achieved for 18 of the 20 amino acids using the precursors $[1-^{13}\text{C}]$ -pyruvate and $\text{NaH}^{13}\text{CO}_3$, the level of labeling is far from desirable for many of the residues. There are clear sensitivity advantages associated with the use of $\text{U}-^{13}\text{C}$ labeled samples that could be exploited if robust measures of chemical shifts can be obtained via relaxation dispersion. In what follows we show that this indeed is the case.

^{13}CO CPMG relaxation dispersion on $\text{U}-^{13}\text{C}$ labeled samples

In a previous set of publications that focused on the $P + L \leftrightarrow PL$ exchanging system that is used here we have shown that accurate ^{13}CO chemical shifts (Hansen et al. 2008c) and ^1HN – ^{13}CO RDCs (Hansen et al. 2008b) could be obtained by relaxation dispersion methods for many residues in selectively labeled samples that were prepared as described above. For example, the chemical shifts of the minor state (corresponding to PL of Eq. 1) were in excellent agreement with those measured directly for Abp1p saturated with Ark1p, with a pair-wise RMSD of 0.02 ppm. Moreover, exchange rates, $k_{\text{ex}} = k_{\text{on}}[L] + k_{\text{off}}$, and populations of the minor state, p_B , could be extracted that agreed well with the corresponding parameters obtained from ^{15}N experiments; $(p_B, k_{\text{ex}}) = (7.5\%, 247 \text{ s}^{-1})$ and $(7.2\%, 263 \text{ s}^{-1})$ from ^{13}CO and ^{15}N experiments, respectively. In order to establish whether accurate ^{13}CO shifts could be obtained from CPMG experiments recorded on uniformly ^{13}C labeled samples, a $\text{U}-^{15}\text{N},^{13}\text{C}$ labeled Abp1p SH3

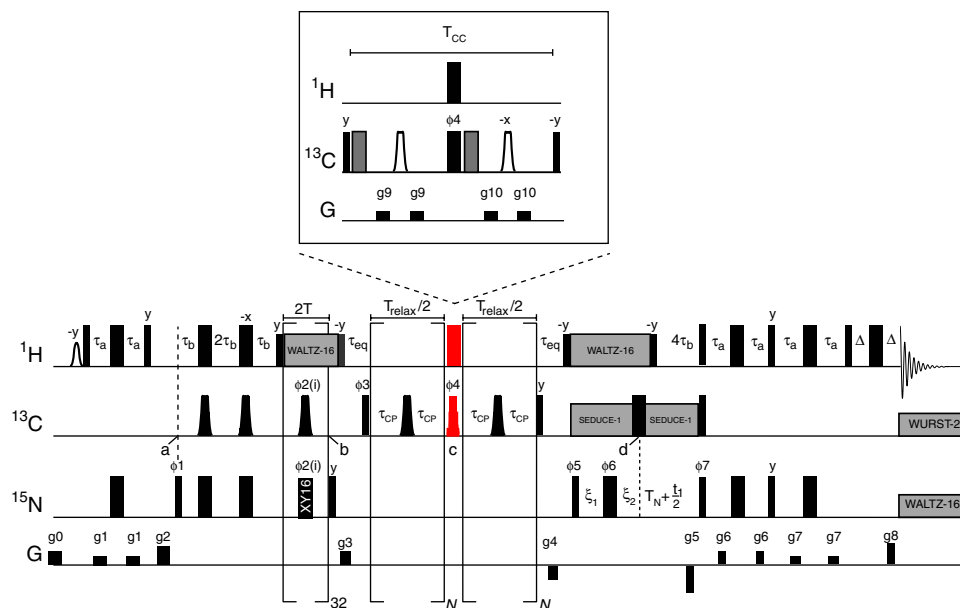


Fig. 2 Pulse scheme of the ^{13}C CPMG relaxation dispersion experiment for measuring millisecond time-scale dynamics in uniformly ^{15}N , ^{13}C -labeled proteins. ^1H , ^{13}C and ^{15}N 90° RF pulses are shown as narrow (wide) bars. In the case of ^{13}C the black, white and gray pulses are centered at 176 (^{13}CO), 58 ($^{13}\text{C}^\alpha$) and 40 ($^{13}\text{C}^\beta$ of Asx) ppm, respectively. The ^1H carrier is placed on the water signal, while the ^{15}N carrier is at 119 ppm. All pulse phases are assumed to be x , unless indicated otherwise. ^1H and ^{15}N pulses as well as the ^{13}C 180° pulse at d are applied at the highest possible power level, while 90° ^{13}C pulses are applied with a field strength of $\Delta\Omega/\sqrt{15}$, where $\Delta\Omega$ is 118 ppm (although higher power pulses could just as well be used). Pulses applied to ^{13}C during the transfer between a and b and during the constant time relaxation period are of duration 450 (380) μs at 600 (800) MHz. These pulses are related to those of the RE-BURP variety (Geen and Freeman 1991) but have been optimized to minimize excitation of magnetization in the aliphatic region of the spectrum (35–85 ppm) and to have a flatter refocusing profile (176 \pm 10 ppm) (see Appendix). Their length limits ν_{CPMG} to values less than ≈ 1 kHz and hence the study of exchange processes to those that are on the order of 1 kHz or less. The shaped 90° ^1H pulse is water-selective (~ 1.6 ms rectangular pulse). Magnetization transfer from ^{15}N to ^{13}CO occurs from a to b . During the initial $4\tau_b$ period ^{15}N magnetization is refocused with respect to ^1H , with concomitant defocusing with respect to ^{13}CO that continues to point b through the application of simultaneous ^{13}C and ^{15}N pulses at a frequency of 800 Hz (i.e., time between successive pulses is $T/16$). This scheme partially quenches chemical exchange that occurs on the millisecond time-scale, leading to improvements in sensitivity (Mulder et al. 1996). The simultaneous pulses (applied as a complete train in each scan) have phases $\phi 2(i) = 2(x, y, x, y, y, x, y, x, -x, -y, -x, -y, -y, -x, -y, -x)$ so that both the x and the y components of transverse magnetization are refocused properly in the presence of off-resonance effects and pulse imperfections (Gullion et al. 1990). ^1H decoupling during the $^{15}\text{N} \rightarrow ^{13}\text{CO}$ transfer and during t_1 is achieved with a WALTZ-16 scheme applied at a field of 6 kHz (Shaka et al. 1983), $^{13}\text{C}^\alpha$ decoupling during t_1 is obtained with the SEDUCE-1 sequence that is cosine modulated with a frequency of

118 ppm (McCoy and Mueller 1992), ^{15}N decoupling during acquisition is achieved with a 1.2 kHz WALTZ-16 scheme, while WURST-2 ^{13}CO decoupling is employed during acquisition to suppress ^1H – ^{13}CO scalar couplings (bandwidth of 12 ppm, centered at 176 ppm, maximum (rms) B_1 field of 0.6 (0.4) kHz) (Kupce and Freeman 1995). The phase cycling used is: $\phi 1 = y, -y, \phi 3 = 2(y), 2(-y), \phi 4 = y, -y, \phi 5 = x, \phi 6 = 4(x), 4(-x), \phi 7 = x$, receiver = $x, -x, -x, x$. The delays used are $\tau_a = 2.25$ ms, $\tau_b = 1/(8J_{\text{NH}}) \sim 1.38$ ms, $\tau_{\text{eq}} = 3$ ms, $T = 10$ ms, $T_{\text{N}} = 13$ ms, $\xi_1 = \max(0, T_{\text{N}} - t_1/2)$, $\xi_2 = \max(0, t_1/2 - T_{\text{N}})$ and $\Delta = 0.5$ ms. In this scheme magnetization is recorded in constant-time mode for $t_1 \leq 2T_{\text{N}}$; subsequently for $t_1 > 2T_{\text{N}}$ signal decays during t_1 creating a discontinuity in the t_1 time domain profile that is similar in some regards to what is obtained in a scheme recently described by Bax and coworkers (Ying et al. 2007). The resulting lineshapes in F_1 have not been problematic in the analysis of any of the data. N is any even or odd number if the sequence is performed without the refocusing element in the inset and any even number if the refocusing element is used. Gradient strengths G/cm (length in ms) are: $g_0 = 8.0(0.5)$, $g_1 = 4.0(0.5)$, $g_2 = 10.0(1.0)$, $g_3 = 7.0(1.0)$, $g_4 = -6.0(0.6)$, $g_5 = -30.0(1.25)$, $g_6 = 4.0(0.3)$, $g_7 = 2.0(0.4)$, $g_8 = 29.6(0.125)$, $g_9 = 3.0(0.3)$, $g_{10} = 6.5(0.4)$. Quadrature detection in the indirect dimension is obtained by recording two sets of spectra with $(\phi 7, g_5)$ and $(\phi 7 + \pi, -g_5)$ for each t_1 increment (Kay et al. 1992; Schleucher et al. 1993); the phase $\phi 5$ and the receiver are incremented by 180° for each complex t_1 point (Marion et al. 1989). The inset shows the refocusing element that partially suppresses the effects of ^{13}CO – ^{13}CO couplings; it replaces the pair of $^1\text{H}/^{13}\text{C}$ pulses at point c in red. The delay $T_{\text{cc}} = 1/J_{\text{C}^\alpha\text{C}^\beta}$ is set to 18.2 ms and the CO – C^α coupling is refocused by C^α selective pulses at $1/4J_{\text{C}^\alpha\text{C}^\beta}$ and $3/4J_{\text{C}^\alpha\text{C}^\beta}$ (RE-BURP pulses (Geen and Freeman 1991) of durations 1450 (1090) μs at 600 (800) MHz, centered at 58 ppm). The gray (black) 180° pulses invert/refocus C^β and CO , respectively, and are applied at a field strength of $\Delta\Omega/\sqrt{3}$, where $\Delta\Omega$ is 136 ppm and centered at 40 and 176 ppm, respectively. The pulse on C^β at the beginning of the element (gray) compensates for the Bloch–Siegert shift (Vuister and Bax 1992)

domain sample with 6.3% bound Ark1p peptide (based on ^{15}N CPMG experiments) was prepared and ^{13}CO relaxation dispersion experiments recorded using the pulse sequence

shown in Fig. 2. This scheme follows very closely ^{13}CO relaxation dispersion experiments that have already been published and described in detail (Hansen et al. 2008c;

Ishima et al. 2004; Vallurupalli et al. 2008a), with minor modifications from our earlier schemes that take into account the fact that experiments are recorded on uniformly ^{13}C —and not selectively labeled—samples. The element shown as an inset to the figure will be described later.

Representative ^{13}CO dispersion profiles recorded at 600 (red) and 800 (blue) MHz are presented in Fig. 3, along with best fits to a global two state exchange process (solid lines). The extracted values of $(p_B, k_{\text{ex}}) = (9.3 \pm 0.04\%, 177 \pm 9 \text{ s}^{-1})$ are quite distinct from values obtained from fits of ^{15}N relaxation dispersion data recorded on the same sample, $(6.3 \pm 0.08\%, 286 \pm 5 \text{ s}^{-1})$. We have shown previously that for this exchanging system the populations and exchange rates are correlated, in a reciprocal fashion, with a χ^2 minimum that is quite shallow (Hansen et al. 2008c). Indeed when the ^{13}CO dispersion data is refit with (p_B, k_{ex}) fixed to those from ^{15}N experiments only a modest increase in the reduced χ^2 was noted, from 0.79 to 0.91.

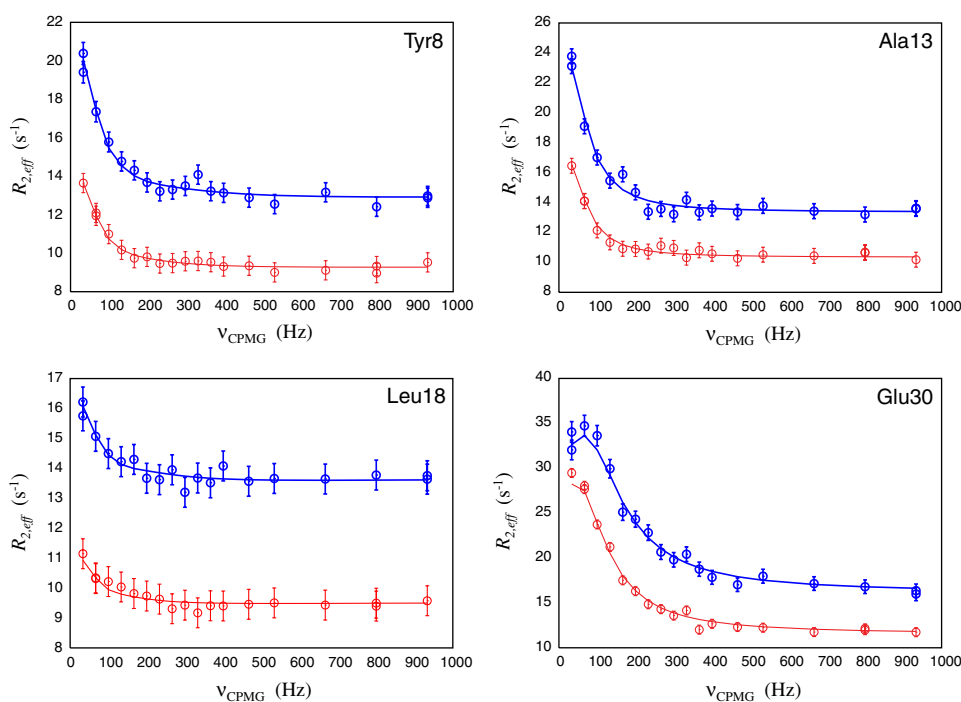
The main goal of the present work is to evaluate the accuracy of ^{13}CO chemical shift differences ($\Delta\varpi$) between pairs of exchanging states that are extracted from fits of dispersion profiles recorded on uniformly ^{13}C labeled samples. Figure 4a compares extracted $\Delta\varpi$ values from CPMG profiles, ($\Delta\varpi_{\text{CPMG}}$; Y axis) with those obtained directly from measurements on apo- and fully saturated SH3 domains ($\Delta\varpi_{\text{Direct}}$; X axis), while Fig. 4b correlates $\Delta\varpi_{\text{CPMG}}$ values from U- ^{13}C labeled ($\Delta\varpi_{\text{CPMG,U}}$; Y axis)

and selectively ^{13}C labeled samples ($\Delta\varpi_{\text{CPMG,S}}$; X axis). It is well known that CPMG experiments do not report the sign of $\Delta\varpi$ and while signs can be obtained by comparing the positions of correlations in (i) HMQC and HSQC experiments recorded at a single field or in (ii) HSQC experiments recorded at two different fields (Skrynnikov et al. 2002), we have not done this here; thus, only $|\Delta\varpi|$ values are compared. As shown in Fig. 4 there is an excellent correlation between $|\Delta\varpi|$ values obtained from CPMG measurements and those based on direct measurements (pair-wise RMSD of 0.02 ppm; maximum difference of 0.05 ppm). Indeed the level of agreement is as good as was obtained from CPMG measurements recorded on samples with ‘isolated’ ^{13}CO spins (Hansen et al. 2008c), establishing that the more sophisticated ^{13}CO selective labeling scheme is not necessary in this case. In fact, there are distinct advantages to uniform labeling that include the fact that (i) exchange can be quantified in the case of Leu and His residues that are not ^{13}C labeled at the carbonyl position using $[1-^{13}\text{C}]$ -pyruvate and $\text{NaH}^{13}\text{CO}_3$ and that (ii) the sensitivity in spectra is significantly improved since the level of ^{13}C incorporation in all CO positions is, of course, close to 100% in U- ^{13}C labeled samples.

Complications from $^3J_{\text{CO,C}}$ in Asx

Ishima and coworkers have carried out simulations that quantify the effects of homonuclear $J_{\text{CO,C}}$ scalar couplings on measured relaxation dispersion profiles for experimental

Fig. 3 ^{13}CO relaxation dispersion profiles recorded on the uniformly ^{13}C labeled Abp1p SH3 domain with $\approx 6\%$ bound peptide, 25°C . Blue (red) symbols indicate data recorded at 800 (600) MHz and the corresponding lines are the best fit to a two state exchange model



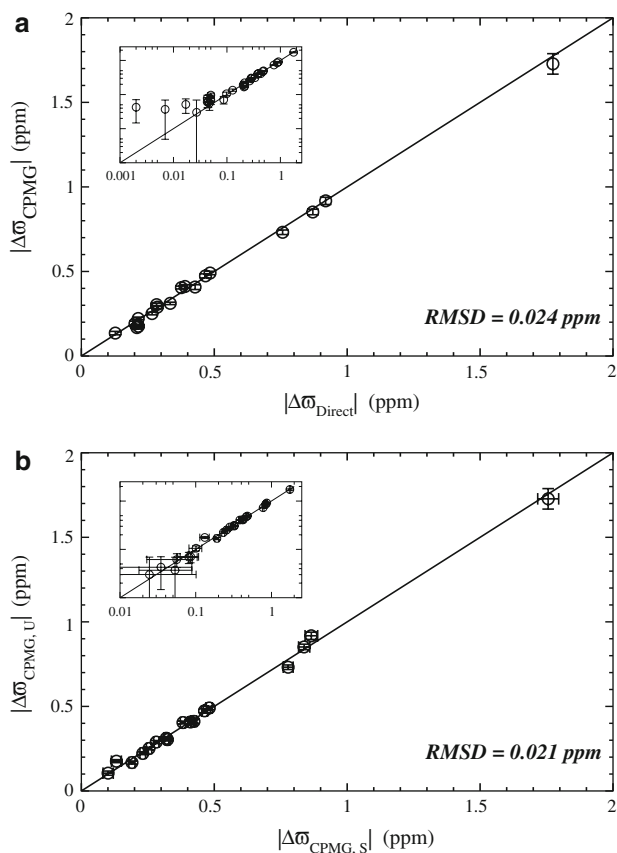


Fig. 4 Correlation between ^{13}C O $|\Delta\sigma|$ values (ppm) extracted from fits of relaxation dispersion data recorded for a uniformly ^{13}C labeled sample and (a) $|\Delta\sigma|$ values obtained from chemical shifts recorded directly (Y axis) on samples of free and fully bound Abp1p SH3 domain or (b) $|\Delta\sigma|$ values extracted from relaxation dispersion data recorded on a selectively ^{13}C O labeled Abp1p SH3 domain sample (Hansen et al. 2008c). The solid lines ($y = x$) would correspond to a perfect correlation between the data sets. Only points for which $|\Delta\sigma| > 0.1$ ppm are retained in the main figures while all data points are shown in the insets as log/log plots. The RMSD between the chemical shifts obtained from each of the compared data sets is indicated in the figure

parameters that are typical for modestly sized proteins (Ishima et al. 2004). Significant artifacts in dispersion profiles can arise for values of $^3J_{\text{CO},\text{C}\gamma}$ that exceed 2–3 Hz; values of $^3J_{\text{CO},\text{C}\gamma}$ in Asx can be as large as 5 Hz for carbonyl groups that are trans (Hu and Bax 1996). Figure 5a, c show dispersion profiles that are recorded for a pair of Asx residues illustrating the characteristic shapes of curves that are generated from significant three bond $^{13}\text{C}\text{O}$ – $^{13}\text{C}\text{O}$ couplings. Quite surprisingly, fits of dispersion profiles of this sort still produce accurate $\Delta\sigma$ values, with errors less than 0.025 ppm for Asx residues (maximum error of 0.04 ppm). This level of accuracy may reflect the fact that for small k_{ex} values of the sort here (200–300 s^{-1}) the exchange information content in the dispersion curve is

‘localized’ to low ν_{CPMG} values (for $\nu_{\text{CPMG}} > k_{\text{ex}}$ the effects of exchange are pulsed out), while the distortions produced from $^3J_{\text{CO},\text{C}\gamma}$ are primarily associated with larger ν_{CPMG} values (>300 Hz).

In an attempt to improve the quality of the dispersion profiles we have developed the pulse scheme shown in the inset to Fig. 2 (referred to in what follows as a J -refocusing element) that replaces the pair of pulses that are in red. Note that the $^{13}\text{C}\text{O}$ pulse of phase ϕ_4 that is replaced leads to refocusing of many of the effects of CPMG pulse imperfections by the end of the CPMG interval, independent of whether N is even (Hansen et al. 2008a). Neglecting the effects of relaxation, the element in the inset also achieves this result (but see below). In order to understand how this element works consider a 2-spin $^{13}\text{C}\text{O}$, $^{13}\text{C}\text{O}$ scalar coupled spin system, ignoring chemical exchange, relaxation and pulse imperfections. Scalar coupling will evolve during the first half of the CPMG interval and in the slow pulsing limit, $\Delta\omega\tau_{\text{CP}} \geq 2.5$, where $\Delta\omega$ is the difference in chemical shifts of the pair of $^{13}\text{C}\text{O}$ spins and $\nu_{\text{CPMG}} = 1/4\tau_{\text{CP}}$, the evolution for $T_{\text{relax}}/2$ can be summarized as,

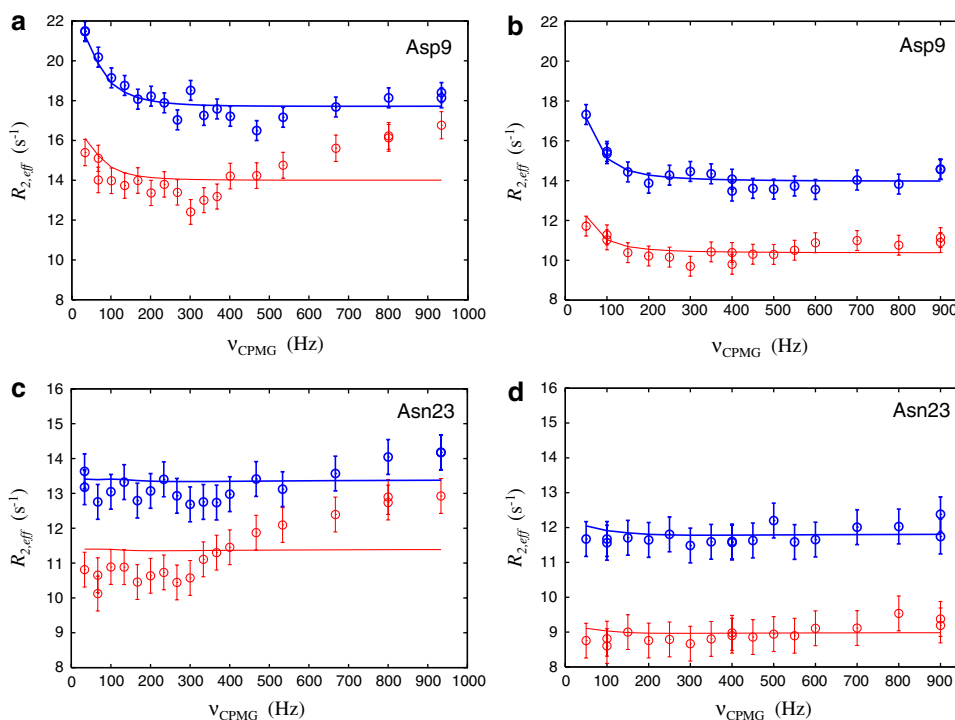
$$\text{CO}_X^A \rightarrow \text{CO}_X^A \cos\left(\pi J_{\text{CO},\text{CO}} \frac{T_{\text{relax}}}{2}\right) + 2\text{CO}_Y^A \text{CO}_Z^B \sin\left(\pi J_{\text{CO},\text{CO}} \frac{T_{\text{relax}}}{2}\right) \quad (2)$$

while in the rapid pulsing limit, $\Delta\omega\tau_{\text{CP}} \leq 1$,

$$\text{CO}_X^A \rightarrow \text{CO}_X^A \cos^2\left(\pi J_{\text{CO},\text{CO}} \frac{T_{\text{relax}}}{2}\right) + \text{CO}_X^B \sin^2\left(\pi J_{\text{CO},\text{CO}} \frac{T_{\text{relax}}}{2}\right) + (\text{CO}_Y^A \text{CO}_Z^B - \text{CO}_Z^A \text{CO}_Y^B) \sin(\pi J_{\text{CO},\text{CO}} T_{\text{relax}}) \quad (3)$$

where superscripts A, B denote backbone and side-chain $^{13}\text{C}\text{O}$ spins, respectively, and the subscripts correspond to the {X, Y, Z} components of magnetization. Application of the first pulse of the J -refocusing element places in-phase X-magnetization along the Z-axis, while anti-phase magnetization is converted into a super-position of double- and zero-quantum coherences that subsequently evolve during the T_{cc} delay due to one bond scalar coupling interactions involving directly coupled aliphatic carbons. Evolution due to $^{13}\text{C}\text{O}^A$ – $^{13}\text{C}^\alpha$ scalar coupling is refocused by the application of $^{13}\text{C}^\alpha$ selective pulses at $0.25T_{\text{cc}}$ and $0.75T_{\text{cc}}$, but evolution due to the one-bond scalar coupling between the side-chain $^{13}\text{C}\text{O}$ ($^{13}\text{C}\text{O}^B$) and its attached $^{13}\text{C}^\beta$ ($J_{\text{CO},\text{C}\beta}$) proceeds during $T_{\text{cc}} = 1/J_{\text{CO},\text{C}\beta}$. The net effect is that immediately after the element, X-magnetization from both $^{13}\text{C}\text{O}^A$ and $^{13}\text{C}\text{O}^B$ is ‘inverted’ ($\text{CO}_X^i \rightarrow -\text{CO}_X^i$, $i \in \{A, B\}$), but not the anti-phase components. A straightforward calculation shows that at the end of the second half of the CPMG interval magnetization is refocused to $-\text{CO}_X^A$. We emphasize that refocusing

Fig. 5 Comparison of dispersion profiles recorded without (a, c) and with (b, d) the $^3J_{\text{CO,CO}}$ refocusing element. Blue (red) symbols indicate data recorded at 800 (600) MHz, 25°C, on a uniformly ^{13}C labeled Abp1p SH3 domain sample ($\approx 6\%$ peptide) and the corresponding lines are the best fit to a two state exchange model. Note that the oscillations in (a, c) are larger for profiles recorded at 600 MHz reflecting the differences in $\Delta\omega$ at the two fields, consistent with expectations based on density matrix simulations of the effects of scalar couplings during CPMG pulse schemes



of $J_{\text{CO,CO}}$ scalar evolution occurs only in the absence of relaxation; it is also the case that refocusing of pulse imperfections during the CPMG train is also compromised by relaxation during the T_{cc} element and we therefore use only even N values with this scheme.

Figure 5 compares dispersion profiles for Asp 9 and Asn 23 that were recorded without (a, c) and with (b, d) the refocusing element that is shown in the inset to Fig. 2. It is clear that the quality of the dispersion profiles has improved with the refocusing element. However, the improved quality of the curves does not translate into more accurate $\Delta\varpi$ values. In the case of the seven Asx residues considered the average pair-wise RMSD of $\Delta\varpi$ from CPMG and direct measures is 0.038 ppm (maximum deviation of 0.06 ppm) when the element in the inset of Fig. 2 is used compared to 0.025 ppm in its absence. For all 31 residues analyzed the average pair-wise RMSD is 0.034 ppm (with J -refocusing) versus 0.024 ppm (without). The increased RMSD with the refocusing element likely reflects the fact that pulse imperfections in the CPMG pulse train are less well compensated and perhaps, to a smaller extent, the decrease in sensitivity of the resultant spectra. Figure 6 illustrates the correlation between extracted $\Delta\varpi$ values from CPMG profiles in the case where the J -refocusing element was employed with shift values obtained directly from measurements on apo- and fully saturated SH3 domains. The level of agreement is still very good (Fig. 6).

In summary we have presented a comparative study of ^{13}C chemical shift differences extracted from relaxation

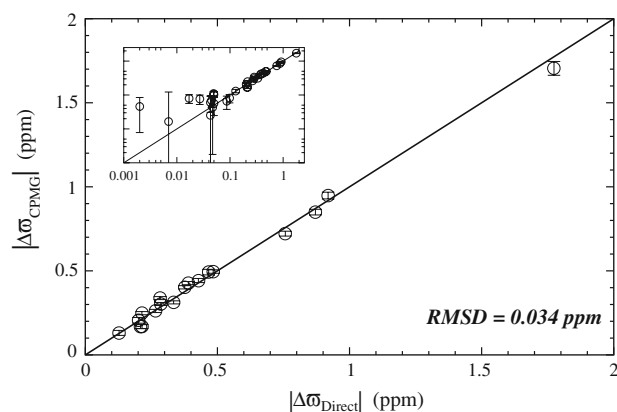
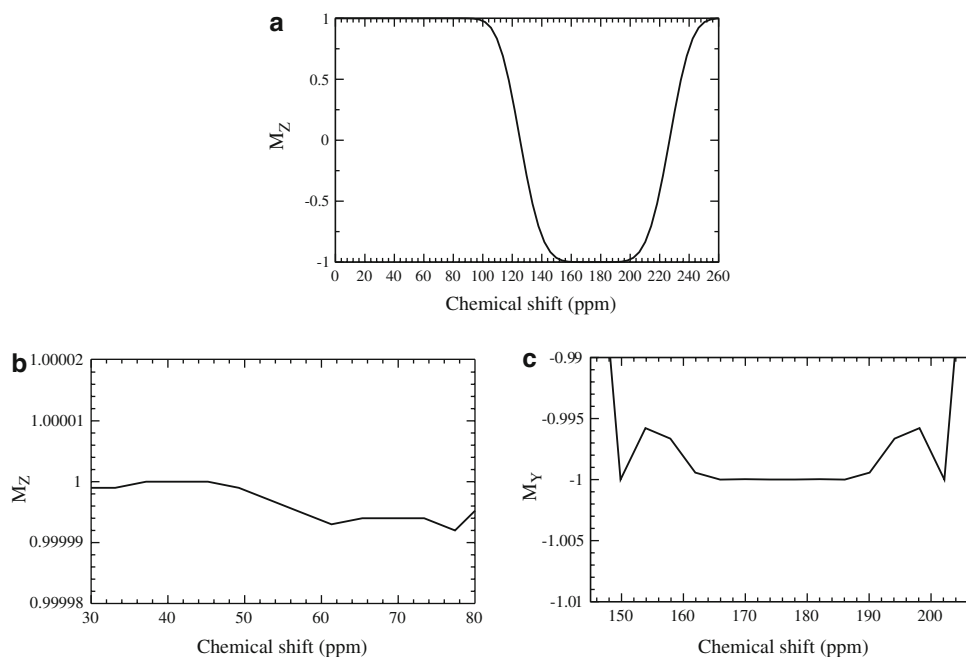


Fig. 6 Correlation between ^{13}C $|\Delta\varpi|$ values (ppm) extracted from fits of relaxation dispersion data recorded on a uniformly ^{13}C labeled Abp1p SH3 domain sample ($\approx 6\%$ peptide) using the version of the pulse sequence of Fig. 2 that includes the $^3J_{\text{CO,CO}}$ refocusing element (Y axis) and the corresponding values measured directly from samples of free and fully bound Abp1p. The solid line ($y = x$) corresponds to a perfect correlation between the two data sets. Only points for which $|\Delta\varpi| > 0.1$ ppm are retained in the main figure while all data points are shown in the inset as a log/log plot. The RMSD between the two data sets is indicated in the figure

dispersion NMR spectra recorded on selectively and uniformly ^{13}C labeled samples. It is shown that accuracy is not sacrificed when using a fully ^{13}C enriched sample. Because the selective labeling approach results in a significant fraction of the residues with ^{13}C label at a level of approximately only 30% (Hansen et al. 2008c), with

Fig. 7 Bloch equation simulations of the effects of the refocusing pulse used in the CPMG experiments on longitudinal and transverse magnetization components. A pulse centered at 176 ppm is used with a maximum field strength of 13.9 kHz and a duration of 450 μ s. The coefficients used to generate the pulse are those given above for 500 MHz. The starting magnetization is $+M_z$ (**a**, **b**) and $+M_y$ (**c**). (**a**) Inversion profile of the pulse. (**b**) Expansion of the region extending from 30 to 80 ppm, showing that perturbation of $^{13}\text{C}^\alpha$ spins is negligible. (**c**) Demonstration of near complete refocusing within the carbonyl chemical shift region



Leu and His not labeled at all, there are decided sensitivity advantages to using a uniformly ^{13}C labeled sample. Although this work has focused on ^{13}CO chemical shifts it seems clear that similarly accurate values will be obtained for ^{13}CO RCSAs (Vallurupalli et al. 2008a) and $^1\text{HN}-^{13}\text{CO}$ RDCs (Hansen et al. 2008b) of the excited state using uniformly labeled samples as well.

Acknowledgments We thank Dr. Elliott Stollar and Ms. Hong Lin for the gift of Ark1p peptide that was used in some of the experiments. This work was supported by a grant from the Canadian Institutes of Health Research (CIHR). P. L. and D. F. H. hold fellowships from the CIHR Training Grant on Protein Folding in Health and Disease (P. L.) and the CIHR (D. F. H.). The authors thank Dr. Pramodh Vallurupalli for useful discussions. L. E. K. is the recipient of a Canada Research Chair in Biochemistry.

Appendix: Description of the ^{13}CO refocusing pulses used in the CPMG element

Pulses are divided into a series of N steps, with the amplitude of step n , $1 \leq n \leq N$ given by

$$\text{amp}_n = \sum_k a_k \cos\left(\frac{2\pi kn}{N+1}\right) / \text{norm} \quad (\text{A1})$$

where $\text{norm} = \sum_k |a_k|$. The phase for each step is x unless the amplitude is negative, in which case the phase is reversed to $-x$ and $|\text{amp}_n|$ is used. Pulses have been optimized for widths of 450 μ s (at 500 and 600 MHz) and 380 μ s (at 800 MHz).

The Fourier coefficients for the ^{13}CO refocusing pulses used in this study are

$a_1 = 0.3867$	0.4896	0.4384
$a_2 = -0.7627$	-0.9913	-0.8904
$a_3 = 0.9219$	1.2505	1.0653
$a_4 = -1.2039$	-1.6490	-1.4168
$a_5 = 0.7780$	0.9791	1.0291
$a_6 = -0.3716$	-0.3213	-0.3350
$a_7 = 0.2337$	0.2233	0.1835
$a_8 = -0.1479$	-0.1577	-0.1560
$a_9 = 0.0966$	0.0982	0.1062
$a_{10} = -0.0682$	-0.0502	-0.0727
$a_{11} = 0.0436$	0.0936	0.0499
$a_{12} = -0.0338$	-0.0924	-0.0342
$a_{13} = 0.0259$	0.0691	0.0260
$a_{14} = -0.0282$	-0.2311	-0.0248
$a_{15} = -0.0643$	0.0915	-0.0122
$a_{16} = 0.0456$	-0.2444	0.1306
$a_{17} = -0.0640$	0.1173	-0.0653
$a_{18} = -0.0116$	-0.1591	-0.0542
$a_{19} = -0.0945$	0.1407	-0.0990
$a_{20} = 0.0201$	-0.1815	0.0857

where columns 1, 2 and 3 list the values for pulses applied at 500, 600 and 800 MHz (code for generating pulses available upon request). The refocusing and inversion profiles are shown in Fig. 7.

References

- Ando I, Saito H, Tabeta R, Shoji A, Ozaki T (1984) Conformation dependent ^{13}C NMR chemical shifts of poly(L-alanine) in the solid state—FPT INDO calculation of *N*-acetyl-*N'*-methyl-L-alanine amide as a model compound of poly(L-alanine). *Macromolecules* 17:457–461
- Bax A (2003) Weak alignment offers new NMR opportunities to study protein structure and dynamics. *Protein Sci* 12:1–16
- Boehr DD, McElheny D, Dyson HJ, Wright PE (2006) The dynamic energy landscape of dihydrofolate reductase catalysis. *Science* 313:1638–1642
- Carr HY, Purcell EM (1954) Effects of diffusion on free precession in nuclear magnetic resonance experiments. *Phys Rev* 94:630–638
- Cavalli A, Salvatella X, Dobson CM, Vendruscolo M (2007) Protein structure determination from NMR chemical shifts. *Proc Natl Acad Sci USA* 104:9615–9620
- Cornilescu G, Delaglio F, Bax A (1999) Protein backbone angle restraints from searching a database for chemical shift and sequence homology. *J Biomol NMR* 13:289–302
- Delaglio F, Grzesiek S, Vuister GW, Zhu G, Pfeifer J, Bax A (1995) NMRPipe—a multidimensional spectral processing system based on unix pipes. *J Biomol NMR* 6:277–293
- Drubin DG, Mulholland J, Zhu ZM, Botstein D (1990) Homology of a yeast actin-binding protein to signal transduction proteins and myosin-I. *Nature* 343:288–290
- Eisenmesser EZ, Bosco DA, Akke M, Kern D (2002) Enzyme dynamics during catalysis. *Science* 295:1520–1523
- Eisenmesser EZ, Millet O, Labeikovsky W, Korzhnev DM, Wolf-Watz M, Bosco DA, Skalicky JJ, Kay LE, Kern D (2005) Intrinsic dynamics of an enzyme underlies catalysis. *Nature* 438:117–121
- Geen H, Freeman R (1991) Band-selective radiofrequency pulses. *J Magn Reson* 93:93–141
- Goddard TD, Kneller DG SPARKY 3, University of California, San Francisco
- Gullion T, Baker DB, Conradi MS (1990) New, compensated Carr–Purcell sequences. *J Magn Reson* 89:479–484
- Hansen AF, Vallurupalli P, Kay LE (2008a) An improved ^{15}N relaxation dispersion experiment for the measurement of millisecond time-scale dynamics in proteins. *J Phys Chem B* 112:5898–5904
- Hansen DF, Vallurupalli P, Kay LE (2008b) Quantifying two-bond ^1HN – ^{13}CO and one-bond $^1\text{H}^\alpha$ – $^{13}\text{C}^\alpha$ dipolar couplings of invisible protein states by spin-state selective relaxation dispersion NMR spectroscopy. *J Am Chem Soc* 130:8397–8405
- Hansen DF, Vallurupalli P, Lundström P, Neudecker P, Kay LE (2008c) Probing chemical shifts of invisible states of proteins with relaxation dispersion NMR spectroscopy: How well can we do? *J Am Chem Soc* 130:2667–2675
- Haynes J, Garcia B, Stollar EJ, Rath A, Andrews BJ, Davidson AR (2007) The biologically relevant targets and binding affinity requirements for the function of the yeast actin-binding protein 1 Src-homology 3 domain vary with genetic context. *Genetics* 176:193–208
- Hill RB, Bracken C, DeGrado WF, Palmer AG (2000) Molecular motions and protein folding: characterization of the backbone dynamics and folding equilibrium of $\alpha_2\text{D}$ using ^{13}C NMR spin relaxation. *J Am Chem Soc* 122:11610–11619
- Hu JS, Bax A (1996) Measurement of three-bond ^{13}C – ^{13}C J couplings between carbonyl and carbonyl/carboxyl carbons in isotopically enriched proteins. *J Am Chem Soc* 118:8170–8171
- Ishima R, Louis JM, Torchia DA (2001) Optimized labeling of (CHD2)- ^{13}C methyl isotopomers in perdeuterated proteins: potential advantages for ^{13}C relaxation studies of methyl dynamics of larger proteins. *J Biomol NMR* 21:167–171
- Ishima R, Baber J, Louis JM, Torchia DA (2004) Carbonyl carbon transverse relaxation dispersion measurements and ms– μs time-scale motion in a protein hydrogen bond network. *J Biomol NMR* 29:187–198
- Kay LE, Ikura M, Tschudin R, Bax A (1990) 3-Dimensional triple-resonance NMR spectroscopy of isotopically enriched proteins. *J Magn Reson* 89:496–514
- Kay LE, Keifer P, Saarinen T (1992) Pure absorption gradient enhanced heteronuclear single quantum correlation spectroscopy with improved sensitivity. *J Am Chem Soc* 114:10663–10665
- Korzhnev DM, Salvatella X, Vendruscolo M, Di Nardo AA, Davidson AR, Dobson CM, Kay LE (2004) Low-populated folding intermediates of Fyn SH3 characterized by relaxation dispersion NMR. *Nature* 430:586–590
- Korzhnev DM, Religa TL, Lundström P, Fersht AR, Kay LE (2007) The folding pathway of an FF domain: characterization of an on-pathway intermediate state under folding conditions by ^{15}N , $^{13}\text{C}^\alpha$ and ^{13}C -methyl relaxation dispersion and $^1\text{H}/^2\text{H}$ -exchange NMR spectroscopy. *J Mol Biol* 372:497–512
- Kupce E, Freeman R (1995) Adiabatic pulses for wide-band inversion and broad-band decoupling. *J Magn Reson Ser A* 115:273–276
- Le HB, Oldfield E (1994) Correlation between ^{15}N NMR chemical shifts in proteins and secondary structure. *J Biomol NMR* 4:341–348
- Lee AL, Urbauer JL, Wand AJ (1997) Improved labeling strategy for ^{13}C relaxation measurements of methyl groups in proteins. *J Biomol NMR* 9:437–440
- LeMaster DM, Kushlan DM (1996) Dynamical mapping of *E. coli* thioredoxin via ^{13}C NMR relaxation analysis. *J Am Chem Soc* 118:9255–9264
- Lila T, Drubin DG (1997) Evidence for physical and functional interactions among two *Saccharomyces cerevisiae* SH3 domain proteins, an adenylyl cyclase-associated protein and the actin cytoskeleton. *Mol Biol Cell* 8:367–385
- Loria JP, Rance M, Palmer AGIII (1999) A relaxation-compensated Carr–Purcell–Meiboom–Gill sequence for characterizing chemical exchange by NMR spectroscopy. *J Am Chem Soc* 121:2331–2332
- Lundström P, Teilum K, Carstensen T, Bezsonova I, Wiesner S, Hansen DF, Religa TL, Akke M, Kay LE (2007) Fractional ^{13}C enrichment of isolated carbons using [1- ^{13}C]- or [2- ^{13}C]-glucose facilitates the accurate measurement of dynamics at backbone C-alpha and side-chain methyl positions in proteins. *J Biomol NMR* 38:199–212
- Marion D, Ikura M, Tschudin R, Bax A (1989) Rapid recording of 2D NMR-spectra without phase cycling—application to the study of hydrogen-exchange in proteins. *J Magn Reson* 85:393–399
- McCoy MA, Mueller L (1992) Selective shaped pulse decoupling in NMR: homonuclear [^{13}C] carbonyl decoupling. *J Am Chem Soc* 114:2108–2112
- Meiboom S, Gill D (1958) Modified spin-echo method for measuring nuclear relaxation times. *Rev Sci Instrum* 29:688–691
- Mihara H, Esaki N (2002) Bacterial cysteine desulfurases: their function and mechanisms. *Appl Microbiol Biotechnol* 60:12–23
- Mulder FAA, Spronk CAEM, Slijper M, Kaptein R, Boelens R (1996) Improved HSQC experiments for the observation of exchange broadened signals. *J Biomol NMR* 8:223–228
- Mulder FAA, Mittermaier A, Hon B, Dahlquist FW, Kay LE (2001) Studying excited states of proteins by NMR spectroscopy. *Nat Struct Biol* 8:932–935
- Mulder FAA, Hon B, Mittermaier A, Dahlquist FW, Kay LE (2002) Slow internal dynamics in proteins: application of NMR relaxation dispersion spectroscopy to methyl groups in a cavity mutant of T4 lysozyme. *J Am Chem Soc* 124:1443–1451
- Neal S, Nip AM, Zhang HY, Wishart DS (2003) Rapid and accurate calculation of protein ^1H , ^{13}C and ^{15}N chemical shifts. *J Biomol NMR* 26:215–240

- Palmer AGIII, Kroenke CD, Loria JP (2001) Nuclear magnetic resonance methods for quantifying microsecond-to-millisecond motions in biological macromolecules. *Method Enzymol* 339:204–238
- Palmer AG, Grey MJ, Wang CY (2005) Solution NMR spin relaxation methods for characterizing chemical exchange in high-molecular-weight systems. *Method Enzymol* 394:430–465
- Pardi A, Wagner G, Wuthrich K (1983) Protein conformation and proton NMR chemical shifts. *Eur J Biochem* 137:445–454
- Prestegard JH, Mayer KL, Valafar H, Benison GC (2005) Determination of protein backbone structures from residual dipolar couplings. *Method Enzymol* 394:175–209
- Rath A, Davidson AR (2000) The design of a hyperstable mutant of the Abp1p SH3 domain by sequence alignment analysis. *Protein Sci* 9:2457–2469
- Schleucher J, Sattler M, Griesinger C (1993) Coherence selection by gradients without signal attenuation—application to the 3-dimensional HNC0 experiment. *Angew Chem Int Edit* 32:1489–1491
- Shaka AJ, Keeler J, Frenkiel T, Freeman R (1983) An improved sequence for broad-band decoupling—WALTZ-16. *J Magn Reson* 52:335–338
- Shen Y, Bax A (2007) Protein backbone chemical shifts predicted from searching a database for torsion angle and sequence homology. *J Biomol NMR* 38:289–302
- Skrynnikov NR, Dahlquist FW, Kay LE (2002) Reconstructing NMR spectra of “invisible” excited protein states using HSQC and HMQC experiments. *J Am Chem Soc* 124:12352–12360
- Spera S, Bax A (1991) Empirical correlation between protein backbone conformation and C^α and C^β ^{13}C nuclear magnetic resonance chemical shifts. *J Am Chem Soc* 113:5490–5492
- Sugase K, Dyson HJ, Wright PE (2007) Mechanism of coupled folding and binding of an intrinsically disordered protein. *Nature* 447:1021–1025
- Teilum K, Brath U, Lundström P, Akke M (2006) Biosynthetic ^{13}C labeling of aromatic side chains in proteins for NMR relaxation measurements. *J Am Chem Soc* 128:2506–2507
- Tjandra N, Bax A (1997) Direct measurement of distances and angles in biomolecules by NMR in a dilute liquid crystalline medium. *Science* 278:1111–1114
- Tollinger M, Skrynnikov NR, Mulder FAA, Forman-Kay JD, Kay LE (2001) Slow dynamics in folded and unfolded states of an SH3 domain. *J Am Chem Soc* 123:11341–11352
- Tolman JR, Flanagan JM, Kennedy MA, Prestegard JH (1995) Nuclear magnetic dipole interactions in field-oriented proteins—information for structure determination in solution. *Proc Natl Acad Sci USA* 92:9279–9283
- Vallurupalli P, Kay LE (2006) Complementarity of ensemble and single-molecule measures of protein motion: a relaxation dispersion NMR study of an enzyme complex. *Proc Natl Acad Sci USA* 103:11910–11915
- Vallurupalli P, Hansen DF, Stollar E, Meirovitch E, Kay LE (2007) Measurement of bond vector orientations in invisible excited states of proteins. *Proc Natl Acad Sci USA* 104:18473–18477
- Vallurupalli P, Hansen DF, Kay LE (2008a) Probing structure in invisible protein states with anisotropic NMR chemical shifts. *J Am Chem Soc* 130:2734–2735
- Vallurupalli P, Hansen DF, Kay LE (2008b) Structures of invisible, excited protein states by relaxation dispersion NMR spectroscopy. *Proc Natl Acad Sci USA* (in press)
- Voet D, Voet JG (1995) *Biochemistry*. Wiley, Hoboken
- Vuister GW, Bax A (1992) Resolution enhancement and spectral editing of uniformly ^{13}C enriched proteins by homonuclear broad band ^{13}C decoupling. *J Magn Reson* 98:428–435
- Wagner G, Pardi A, Wuthrich K (1983) Hydrogen bond length and ^1H NMR chemical shifts in proteins. *J Am Chem Soc* 105:5948–5949
- Wand AJ, Bieber RJ, Urbauer JL, McEvoy RP, Gan ZH (1995) Carbon relaxation in randomly fractionally ^{13}C -enriched proteins. *J Magn Reson Ser B* 108:173–175
- Watt ED, Shimada H, Kovrigin EL, Loria JP (2007) The mechanism of rate-limiting motions in enzyme function. *Proc Natl Acad Sci USA* 104:11981–11986
- Wishart DS, Case DA (2002) Use of chemical shifts in macromolecular structure determination. *Method Enzymol* 338:3–34
- Wishart DS, Sykes BD (1994) The ^{13}C chemical-shift index—a simple method for the identification of protein secondary structure using ^{13}C chemical-shift data. *J Biomol NMR* 4:171–180
- Wishart DS, Sykes BD, Richards FM (1991) Relationship between nuclear magnetic resonance chemical shift and protein secondary structure. *J Mol Biol* 222:311–333
- Wolf-Watz M, Thai V, Henzler-Wildman K, Hadjipavlou G, Eisenmesser EZ, Kern D (2004) Linkage between dynamics and catalysis in a thermophilic-mesophilic enzyme pair. *Nat Struct Mol Biol* 11:945–949
- Xu XP, Case DA (2002) Probing multiple effects on ^{15}N , $^{13}\text{C}^\alpha$, $^{13}\text{C}^\beta$, and $^{13}\text{C}'$ chemical shifts in peptides using density functional theory. *Biopolymers* 65:408–423
- Ying JF, Chill JH, Louis JM, Bax A (2007) Mixed-time parallel evolution in multiple quantum NMR experiments: sensitivity and resolution enhancement in heteronuclear NMR. *J Biomol NMR* 37:195–204
- Zeeb M, Balbach J (2005) NMR spectroscopic characterization of millisecond protein folding by transverse relaxation dispersion measurements. *J Am Chem Soc* 127:13207–13212